Structure Determination of the α = 3, β = 6 Term of the $(A_3B_2O_6)_\alpha(A_3B_3O_9)_\beta$ Homologous Series (A = Ba, B = Rh) by a Combination of Powder X-ray Diffraction and Electron Microscopy

Khalid Boulahya,[a] María Hernando,[a] Aurea Varela,[a] José M. González-Calbet,*[a] Marina Parras,[a] Ulises Amador,[b] and José L. Martínez[c]

Keywords: One-dimensional oxides / X-ray diffraction / Electron diffraction / Electron microscopy

The α = 3, β = 6 term of the series $(A_3B_2O_6)_\alpha$ $(A_3B_3O_9)_\beta$ has been synthesized in polycrystalline form. The structural characterization by powder X-ray diffraction, electron diffraction and high-resolution electron microscopy indicates that this material is isostructural with $Ba_9Co_8O_{24}$. In the structure, seven face-sharing octahedra alternate with a trigonal prism defining chains running parallel to the *c* axis of a rhombohedral unit cell ($R\bar{3}c$), with parameters a = 1.00766(4) nm and c = 4.1571(2) nm. The structural refinement shows the presence of a small percentage of Rh vacancies leading to the composition $Ba_9Rh_{7.92}O_{24}$. Pauli paramagnetic behaviour is observed.

Introduction

Recently, a great deal of interest has been devoted to a family of pseudo-monodimensional oxides structurally related to the 2H-hexagonal perovskite ABO_3.[1] This structure and the K_4CdCl_6 structure type[2] constitute the two end-members of this family. The main feature of both structures is that they are formed by a hexagonal array of isolated chains of face-sharing polyhedra running parallel to the *c* axis. In the hexagonal 2H-ABO_3 perovskite, the polyhedral rows are built up by $[BO_6]$ octahedra (O_h), while in the K_4CdCl_6 halide, or $A_3A'BO_6$ oxide,[3] one $[BO_6]$ octahedron and one $[A'O_6]$ trigonal prism (TP) alternate in an ordered 1:1 sequence. An unlimited number of closely related structures can be generated by varying the ratio of the octahedral and trigonal prisms.

There are several ways to describe this family of materials. Darriet et al.[4] provide a structural systematisation of these phases based on the stacking of $[A_3O_9]$ and $[A_3A'O_6]$ layers. The B and A′ cations fill the generated O_h and TP sites, respectively. Different sequences of both layer types lead to different stoichiometries that can be expressed by the general formula $A_{3n+3m}A'_nB_{3m+n}O_{9m+6n}$. Besides this generic formulation, several general formulas have been proposed to denote this homologous series, and different approaches to describe their structures have been reported.[5−7] A very useful approach is to consider these structures as formed by the ordered intergrowth of the structural units building up the two end-members. This building principle gives rise to the $(A_3A'BO_6)_\alpha(A_3B_3O_9)_\beta$ general formula,[8] where α and β denote the number of $A_3A'BO_6$ and 2H-ABO_3 structural blocks in each member, respectively.

A large number of one-dimensional oxides have been obtained by varying the chemical nature of A, A′ and B cations in the above family, due to the ability of these structures to accommodate any value of α and β blocks. So far, when A′ = B, few oxides have been reported and members belonging to this family have been only described in the A-(A′ = B)-O (A = Ca, Sr, Ba; B = Co, Ni, Rh) systems. Among them, the A-Co-O system has proven to be the most fruitful one: at least twelve members of the above series have been stabilized by varying the chemical nature of the alkaline-earth metal between the two limiting structures $Ca_3Co_2O_6$ (α = 3,β = 0)[9] and 2H-$BaCoO_3$ [10] (α = 0, β = 3).[8,11,12] In all of them, cobalt atoms occupy both the TP and the O_h sites. It is worth mentioning that $Ba_9Co_8O_{24}$,[11] the α = 3, β = 6 member, is, apart from the end-member of this series, the largest member of this one-dimensional family stabilized until now. In this phase, seven octahedra and one trigonal prism constitute the polyhedral chains by sharing faces.

When Ni occupies the polyhedral chains, the stabilized phases are much less numerous. The α = 3, β = 1 term $Sr_4Ni_3O_9$,[13] the α = 2, β = 1 term $Sr_9Ni_7O_{21}$,[14] and the

[a] Departamento de Química Inorgánica, Facultad de Químicas, Universidad Complutense
28040 Madrid, Spain
E-mail: jgcalbet@quim.ucm.es
[b] Departamento de Química Inorgánica y Materiales, Facultad de Ciencias Experimentales y Técnicas, Universidad San Pablo, Urb. Montepríncipe, Boadilla del Monte
28668 Madrid, Spain
[c] Instituto Ciencia de Materiales, CSIC, Cantoblanco, 28049, Madrid, Spain

$\alpha = 3$, $\beta = 3$ term $Ba_6Ni_5O_{15}$ [15] have been synthesised and structurally characterized.

Finally, when $A' = B = Rh$, only a 1D-oxide has been described: Zur Loye et al.[16] reported the stabilization of the $Sr_6Rh_5O_{15}$ phase, closely related to $Sr_6Co_5O_{15}$,[17] the $\alpha = 3$, $\beta = 3$ member of the above series. In fact, the main structural features of the latter are maintained in the Sr-Rh oxide, i.e. the polyhedral rows are also constituted by four face-sharing RhO_6 octahedra linked by one RhO_6 trigonal prism. However, when Rh occupies these polyhedra, the authors propose, from X-ray diffraction data, a new unit cell doubling the basal plane with respect to the $Sr_6Co_5O_{15}$ oxide. This superstructure seems to originate from a distortion of the strontium chains. The microstructural characterization[18] of such a member shows that it actually presents a complex stoichiometry, $Sr_{30}Rh_{23}O_{75}$, which results from the presence of empty Rh sites in the polyhedral chains. This feature leads to a fivefold superstructure along the *c* axis with respect to the $Sr_6Co_5O_{15}$ unit cell.

In the Ba-Rh-O system, several well-known ABO_3-hexagonal polytypes have been described. The hexagonal 4H[19] and 18R-$BaRhO_3$ [20] phases can be stabilized under oxidising conditions. These hexagonal phases, which always present the Ba/Rh = 1:1 cationic ratio, can be structurally considered as intermediates between the cubic-ABO_3 perovskite and the 2H-type, hexagonal-ABO_3 perovskite. The latter structure therefore provides the link between these phases and the monodimensional oxides belonging to the $(A_3A'BO_6)_\alpha(A_3B_3O_9)_\beta$ family. Much less information on these rhodium-containing phases is available, since only the synthesis of a non-commensurate $Ba_{1.06}RhO_3$ single crystal has been reported, and no structural data were provided.[21]

In a systematic characterization of powdered samples in the A-Rh-O system (A = Sr, Ba),[22,23] preliminary data from selective area electron diffraction (SAED) and high-resolution electron microscopy (HREM) give evidence of a commensurate one-dimensional Ba-Rh oxide belonging to the $(A_3A'BO_6)_\alpha(A_3B_3O_9)_\beta$ family with the composition $Ba_9Rh_8O_{24}$. We describe in this paper its synthesis and structural characterization by means of X-ray and electron diffraction and HREM. This study reveals that this new oxide adopts the structure corresponding to the $\alpha = 3$, $\beta = 6$ member of the series and, therefore, that it is isostructural to $Ba_9Co_8O_{24}$. $Ba_9Rh_8O_{24}$ is therefore the second such example reported, expanding the range of elements that can be incorporated into this structure. (NB During the writing of this paper, Slitzer et al.[24] reported the structure determination of a $Ba_9Rh_8O_{24}$ single crystal. Both powder and single crystal X-ray diffraction data provide structural models that are coincident in the main features.)

Results and Discussion

Chemical and Structural Characterization

The sample of nominal composition $Ba_9Rh_8O_{24}$ was confirmed to be a single phase by X-ray diffraction (XRD). The average Ba:Rh ratio, as determined by ICP, is close to 0.90(5) along the whole sample, in good agreement with the nominal metallic ratio. It is worth emphasizing that energy dispersive spectroscopy (EDS) analyses performed on numerous crystallites suggest that the sample is very homogeneous, since all of them exhibit the same Ba/Rh ratio of close to 0.9, confirming the ICP results. The anionic composition, as determined from TGA data, is in agreement with 24 oxygen atoms per formula unit, indicating that the anionic sublattice is complete.

The whole XRD pattern of $Ba_9Rh_8O_{24}$ (Figure 1) can be indexed within a hexagonal unit cell of parameters $a = 1.00755(7)$ nm and $c = 4.1572(3)$ nm, corresponding to the $\alpha = 3$, $\beta = 6$ member of the $(A_3B_2O_6)_\alpha(A_3B_3O_9)_\beta$ family.

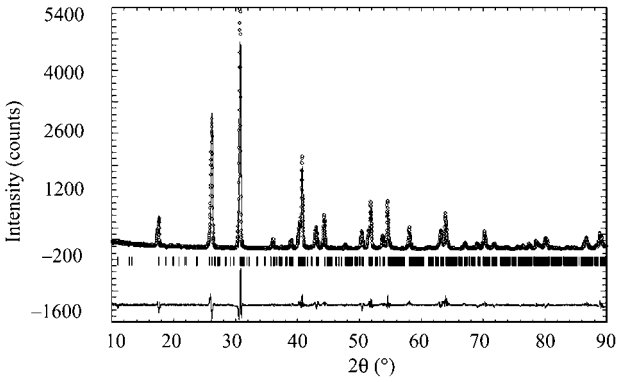

Figure 1. Results of the fitting of the powder XRD data of $Ba_9Rh_{7.92}O_{24}$: experimental (points), calculated (solid line) and difference (bottom)

Microstructural characterization by SAED and HREM confirms the XRD results. The most relevant SAED patterns, taken along the $[\bar{2}110]$, [0001] and $[1\bar{1}00]$ zone axes are shown in Figure 2a, 2b and 2c, respectively. Among them, the $[\bar{2}110]$ reciprocal plane provides the most valuable structural information. In fact, this SAED pattern allows us to obtain directly the values of α and β structural blocks forming the corresponding structure, and, thus, to identify the different members of the $(A_3B_2O_6)_\alpha(A_3B_3O_9)_\beta$ series. For this purpose, it is useful to describe this SAED pattern on the basis of the 2H-hexagonal subcell by differencing two sets of maxima. The more intense spots (referred to as subindex 2H in Figure 2a) correspond to the hexagonal 2H planes, while the least intense ones can be considered as satellite reflections with a modulation vector $\mathbf{k} = (a^*_{2H} + b^*_{2H})/3 + m\,2c^*_{2H}$. The *z* component (*m*) of this vector is related to the α and β values according to the expression $m = \alpha/(3\alpha + 3\beta)$. Besides, and taking into account that such a modulation is commensurate, the studied $Ba_9Rh_8O_{24}$ phase can also be regarded as a 2H superstructure, the 2H superstructure direction being $[\alpha+\beta\ \alpha+\beta\ i\ 2\alpha]^*_{2H}$. In this case, as can be observed in Figure 2a, this direction corresponds to $[33\bar{6}2]_{2H}$, and the *m* value is 1/9, therefore the $\alpha = 3$, $\beta = 6$ values are obtained, which indicates the stabilization of such a member in the Ba-Rh-O system. Furthermore, the observed reflection conditions, (*hkl*), $-h+k+l = 3n$, (000*l*) $l = 6n$ and (*h*00) $h = 3n$, are in agreement with

the rhombohedral $R\bar{3}c$ space group previously proposed for the $Ba_9Co_8O_{24}$ oxide.[11]

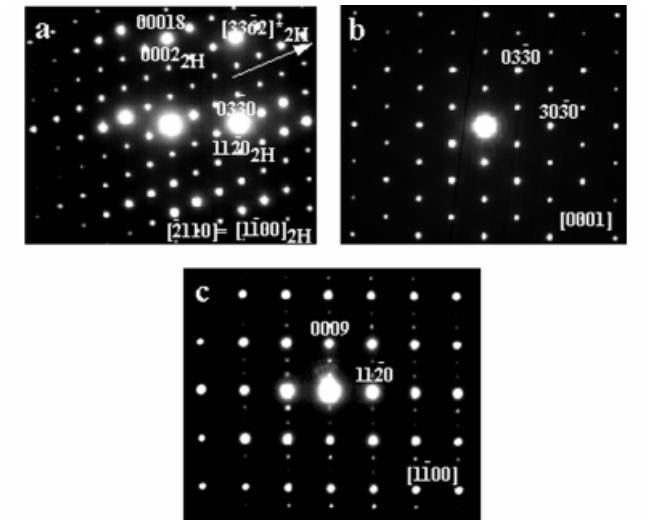

Figure 2. SAED patterns corresponding to $Ba_9Rh_{7.92}O_{24}$ along the [$\bar{2}$110] (a), [0001] (b) and [1$\bar{1}$00] (c) zone axes

The SAED patterns shown in Figure 2b and 2c confirm this result. In the first one, along the [0001] reciprocal plane, the reflections are distributed in a hexagonal array corresponding to a lattice parameter close to 1.0 nm. Only the (*h00*), *h* = *3n* reflections are visible according to the $R\bar{3}c$ space group. Furthermore, the [1$\bar{1}$00] reciprocal plane is also in agreement with the rhombohedral unit cell of this phase, although (*000l*), *l* = 3n reflections appear due to the dynamical diffraction effect.

The polyhedral sequence along the *c* axis, i.e. the arrangement of the blocks building the structure, can be deduced from the contrast variation observed in the experimental HREM. Figure 3 shows the high-resolution micrograph of the $Ba_9Rh_8O_{24}$ compound along the [$\bar{2}$110] zone axis. An apparently well-ordered material is observed with d-spacings close to 2.05 and 0.87 nm, corresponding to d_{002} and d_{100} of the hexagonal unit cell obtained by XRD. The image features are very close to those found in $Ba_9Co_8O_{24}$ and can be interpreted in a similar way. The sequence of bright dots of different contrast is due to rhodium columns. The two brightest dots correspond to the Rh prisms that are aligned following the diagonal cell, according to the rhombohedral symmetry proposed for this phase. The less intense dots could be due to Rh in an octahedral environment, leading to the -1TP-7O_h- polyhedra sequence characteristic of this structure. From this ideal model, the image has been calculated using the MacTempas package. The simulated image (inset in Figure 3) fits well with the experimental one for Δf = −95 nm and a sample thickness of 6 nm.

These results when taken together allow us to conclude that $Ba_9Rh_8O_{24}$ is isostructural to $Ba_9Co_8O_{24}$ and, therefore, that rhodium metal can also be incorporated into the metal-oxygen structure framework of the α = 3, β = 6 member of the one-dimensional $(A_3B_2O_6)_\alpha(A_3B_3O_9)_\beta$ family.

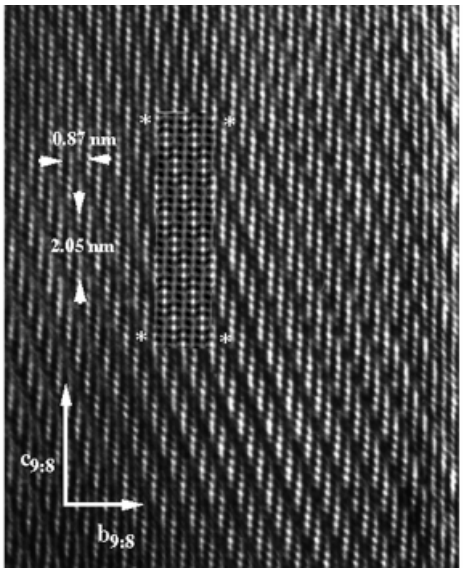

Figure 3. HREM image of $Ba_9Rh_{7.92}O_{24}$ along the [$\bar{2}$110] axis; the simulated image (Δf = −95 nm, Δf = 6 nm) is shown at the inset

Structural Refinement

Since the previous structural results obtained from SAED and HREM data suggested that the title compound is isostructural to $Ba_9Co_8O_{24}$, the structure of the latter was used as the starting model for the refinement of the XRD data of $Ba_9Rh_8O_{24}$. Figure 1 shows the graphic result of the fitting of the experimental X-ray diffraction pattern for $Ba_9Rh_8O_{24}$ and the difference between observed and calculated data. The final structural parameters are collected in Table 1; Table 2 shows some selected interatomic distances. A schematic representation of the structure is depicted in Figure 4a.

Table 1. Final structural parameters of $Ba_9Rh_{7.92}O_{24}$ [a]

Atom	x/a	y/b	z/c	Occ.
Ba(1)	0.3232(9)	−0.007(1)	0.0264(1)	1.000(2)
Ba(2)	0.351(1)	0	1/4	1.000(1)
Rh(1)	0	0	1/4	1.000(2)
Rh(2)	0	0	0.1826(3)	1.000(1)
Rh(3)	0	0	0.1206(4)	0.999(1)
Rh(4)	0	0	0.0618(4)	0.96(1)
Rh(5)	0	0	0	1.000(2)
O(1)	0.171(5)	0.178(5)	0.029(2)	1
O(2)	0.682(6)	0.177(5)	0.049(1)	1
O(3)	0.507(6)	0.353(6)	0.245(2)	1
O(4)	0.364(5)	0.517(6)	0.012(1)	1

[a] Space group $R\bar{3}c$ (167), *a* = 1.00766(4) nm, *c* = 4.1571(2) nm, *V* = 3.6556(2) nm^3, $B_{overall}(A^2)$ = 0.97(4), R_B = 0.075, R_{exp} = 0.086, R_{wp} = 0.16, χ^2 = 3.4.

As is well-known, X-ray diffraction is not the best technique to study structural effects related to light atoms such as oxygen in a "matrix" of heavy metallic atoms, as is the case with our material. In the diffraction pattern of these

Table 2. Selected inter-atomic distances (Å) in $Ba_9Rh_{7.92}O_{24}$

Ba(1)−O(1)	2.95(6)	Rh(1)−O(1)	2.18(5) × 6
Ba(1)−O(1)′	2.76(6)		
Ba(1)−O(1)"	2.77(8)	Rh(2)−O(2)	2.16(5) × 3
Ba(1)−O(2)	3.00(4)	Rh(2)−O(4)	2.04(5) × 3
Ba(1)−O(3)	2.72(6)		
Ba(1)−O(3)′	3.00(7)	Rh(3)−O(3)	2.19(7) × 3
Ba(1)−O(4)	2.74(6)	Rh(3)−O(4)	2.19(6) × 3
Ba(1)−O(4)′	2.42(5)		
		Rh(4)−O(1)	2.22(7) × 3
Ba(2)−O(1)	2.72(8) × 2	Rh(4)−O(3)	2.03(6) × 3
Ba(2)−O(2)	2.36(6) × 2		
Ba(2)−O(3)	2.59(7) × 2	Rh(5)−O(1)	2.13(6) × 6
Ba(2)−O(3)′	3.10(6) × 2		
Rh(1)−Rh(2)	2.80(1)		
Rh(2)−Rh(3)	2.58(2)		
Rh(3)−Rh(4)	2.45(2)		
Rh(4)−Rh(5)	2.57(2)		

one-dimensional materials, a strong preferred orientation effect is usually present because of the pronounced hexagonal shape of the crystallites. This is an additional problem when it comes to solving and refining the structure of these materials from powder diffraction data. In spite of this, the refinement was stable and it was possible to refine the positions of the oxygen atoms, provided an overall temperature factor was used. Any attempt to use individual temperature factors yielded unstable refinements, probably due to the very large volume of the cell and the limited number of observed reflections. Thus, the metal−oxygen distances in Table 2 should be considered with some care, although the metallic coordination, i.e. the polyhedron defined by the closest oxygen atoms around a given metal, is undoubtedly correct. According to that, both Ba atoms are coordinated to eight oxygen atoms at distances in the range 2.36−3.02 Å. Rh(1) occupies a regular trigonal prism, while the other Rh atoms (2, 3, 4 and 5) are octahedrally coordinated by nearby oxygen atoms at the distances reported in Table 2. The obtained values for all M−O distances are reasonable and consistent with previously reported bond lengths in comparable Ba/Rh oxides.[20,21]

Inside the chains, the inter-octahedral Rh(2)−Rh(3) and Rh(4)−Rh(5) distances are very close to those found in 4H or 18H-$BaRhO_3$ (2.5−2.6 Å). However, the Rh(3)−Rh(4) distance (2.45 Å) is significantly shorter and this could be due to the presence of some Rh vacancies in the Rh(4) octahedral site. On the other hand, the distance between Rh(1) in a trigonal prism and Rh(2) in a neighbouring octahedron sharing a triangular face is larger than the other Rh−Rh distances (2.81 Å). Although there is no comparable data for Rh ions in a similar oxygen environment, the enlargement of the distance between TP-O_h metals compared to that shown by O_h-O_h metals is also observed in other similar one-dimensional oxides such as $Ba_6Ni_5O_{15}$ [16] and $Sr_6Co_5O_{15}$.[17]

It is worth mentioning that we found some degree of metal vacancies (4%) in one of the rhodium positions. According to this, the actual composition of the title material

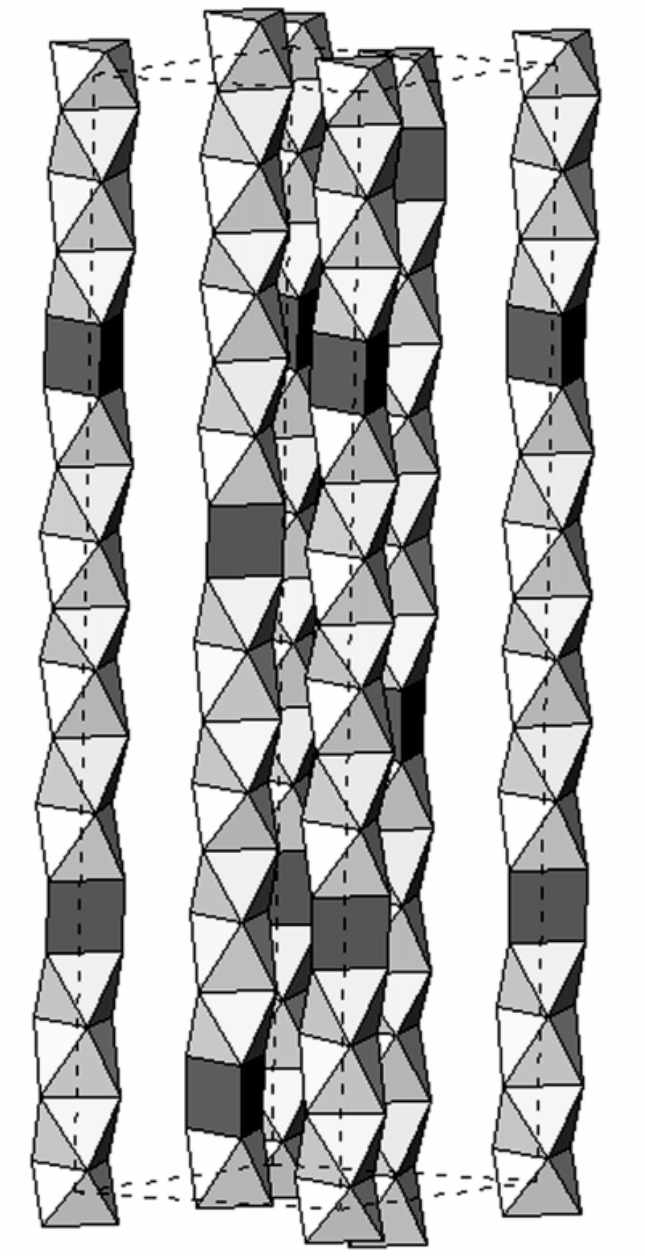

Figure 4. Schematic representation of the $Ba_9Rh_{7.92}O_{24}$ structure; Ba atoms have been omitted for clarity

obtained from the refinement of XRD data is $Ba_9Rh_{7.92(2)}O_{24}$. Assuming the usual valences for Ba and O, then the average Rh oxidation state is +3.78, indicating the presence of both Rh^{IV} and Rh^{III} in the polyhedra chains. However, Bond Valence Sums (BVS) calculations[25] give inappropriate values of the actual oxidation states of rhodium atoms.

The presence of vacancies at rhodium positions seems to play an important role in the stabilisation of the structures. In fact, as we have mentioned above, the $\alpha = 3$, $\beta = 3$ member of this series, stabilised when Sr fully occupies the A-sublattice, is characterized by the presence of one empty position every ten Rh sites in the polyhedra rows. The or-

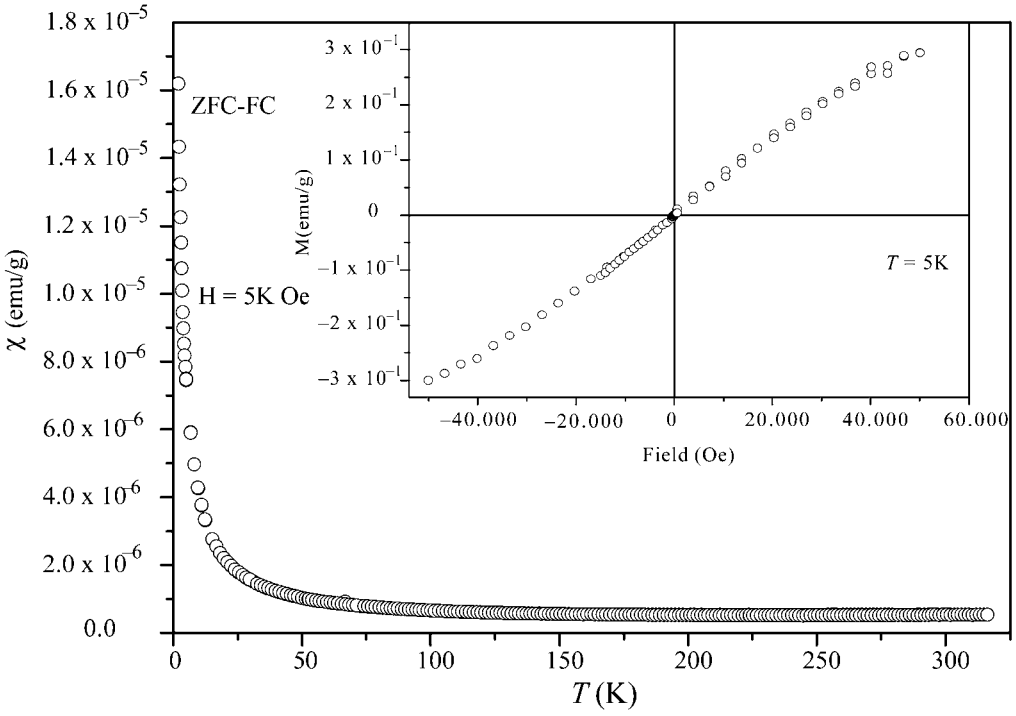

Figure 5. Magnetic susceptibility versus temperature plot for polycrystalline $Ba_9Rh_{7.92}O_{24}$; the susceptibility variation as a function of the applied field is shown as the inset

dered distribution of empty and full sites along the crystal is clearly seen in both the SAED patterns and the HREM study. Interestingly enough, the Rh vacancy concentration in $Ba_9Rh_{7.92}O_{24}$ is considerably lower, and it is not detected either by SAED or HREM. Apparently, the substitution of Sr by Ba causes an increase of the polyhedra average volume in such a way that Rh^{III} can also be accommodated into the structure and, therefore, the number of empty sites decreases considerably.

Magnetic Behaviour

Figure 5 shows the variation of the magnetic susceptibility versus temperature for $Ba_9Rh_{7.92}O_{24}$. The magnetic susceptibility of this oxide presents a Pauli-type behaviour, with an almost temperature independent susceptibility in a wide temperature range from 100 K to 350 K. At low temperature, the susceptibility shows a Curie tail which may be due to a small paramagnetic contribution. A low temperature isotherm until 5T (inset of Figure 5) shows an almost linear behaviour as expected for a Pauli-like system. From the magnetic point of view the system appears to be a linear chain of Rh^{IV} atoms with uncoupled electrons.

Experimental Section

Polycrystalline $Ba_9Rh_8O_{24}$ was prepared by a solid-state reaction with stoichiometric amounts of $BaCO_3$ (Merck, 99.9%) and RhO_2 (Aldrich, 99.8%). The mixture was initially calcined at 900 °C for 12 hours, and then heated at 1050 °C for three days.

The average cationic composition was determined by Inductively Coupled Plasma (ICP) while the local composition in every crystal was analysed by X-ray Energy Dispersive Spectroscopy (EDS). For this purpose, a JEOL 2000 FX electron microscope equipped with a LINK ISIS 300 analyser system was employed. The oxygen content was determined by thermogravimetric analysis (TGA) by using a thermobalance based on a CAHN D-200 electrobalance. The sample (about 100 mg) was reduced in a platinum crucible at 700 °C under $0.2H_2/0.3He$ atmosphere.

Powder X-ray diffraction (XRD) patterns were collected at room temperature on a PHILIPS X′PERT diffractometer equipped with a graphite monochromator and Cu-K_α radiation. The diffraction data were analysed by the Rietveld method[26] using the Fullprof program.[27]

Selected Area Electron Diffraction (SAED) was carried out using a JEOL 2000FX electron microscope fitted with a double-tilting goniometer stage (±45°). High Resolution Electron Microscopy (HREM) was performed on a JEOL 4000EX electron microscope fitted with a double-tilting goniometer stage (±25°). Simulated HREM images were calculated by the multi-slice method using the MacTempas software package.

Magnetic behaviour was measured by a SQUID magnetometer in a temperature range from 5 to 350 K, with a maximum applied magnetic field of 5T.

Acknowledgments

Financial support through research project MAT98-0648 (CICYT, Spain) is acknowledged.

[1] J. J. Lander, *Acta Crystallogr.* **1951**, *4*, 148−156.
[2] G. Bergerhoff, O. Schmitz-Dumont, *Z. Anorg. Allg. Chem.* **1956**, *284*, 10−14.
[3] J. J. Randall, L. Katz, *Acta Crystallogr.* **1959**, *12*, 148−151.
[4] J. Darriet, M. A. Subramanian, *J. Mater. Chem.* **1995**, *5*, 543−552.
[5] M. Evain, F. Boucher, O. Gourdon, V. Petricek, M. Dusek, P. Bezdicka, *Chem. Mater.* **1998**, *10*, 3068−76.
[6] J. M. Perez-Mato, M. Zakhour-Nakhl, F. Weill, J. Darriet, *J. Mater. Chem.* **1999**, *9*, 2795−2808.
[7] K. Ukey, A. Yamamoto, Y. Watanabe, T. Shishido, T. Fukuda, *Acta Crystallogr., Sect. B* **1993**, *49*, 67−72.
[8] K. Boulahya, M. Parras, J. M. González-Calbet, *Chem. Mater.* **2000**, *12*, 25−32.
[9] H. Fjellvag, E. Gulbrandsen, S. Aasland, A. Olsen, B. Hauback, *J. Solid State Chem.* **1996**, *124*, 190−194.
[10] H. Taguchi, Y. Takeda, F. Kanamara, M. Shimada, M. Kaizumi, *Acta Crystallogr., Sect. B* **1977**, *33*, 1299−1301.
[11] K. Boulahya, M. Parras, J. M. González-Calbet, *J. Solid State Chem.* **1999**, *142*, 419−427.
[12] K. Boulahya, M. Parras, J. M. González-Calbet, *J. Solid State Chem.* **1999**, *145*, 116−127.
[13] M. Huvé, C. Renard, F. Abraham, G. Van Tendeloo, S. Amelinckx, *J. Solid State Chem.* **1998**, *135*, 1−16.
[14] J. Campá, E. Gutierrez-Puebla, A. Monge, I. Rasines, C. Ruiz-Valero, *J. Solid State Chem.* **1996**, *126*, 27−32.
[15] J. Campá, E. Gutierrez-Puebla, A. Monge, I. Rasines, C. Ruiz-Valero, *J. Solid State Chem.* **1994**, *108*, 230−235.
[16] J. B. Claridge, H.-C. zur Loye, *Chem. Mater.* **1998**, *10*, 2320−2322.
[17] W. T. A. Harrison, S. L. Hagwood, A. J. Jacobson, *J. Chem. Soc., Chem. Commun.* **1995**, 1953−1954.
[18] A. Varela, K. Boulahya, M. Parras, J. M. Gonzalez-Calbet, *Chem. Mater.* **2000**, *12*, 3237−3239.
[19] B. L. Chamberland, J. B. Anderson, *J. Solid State Chem.* **1981**, *39*, 114−119.
[20] T. Siegrist, E. M. Larson, B. L. Chamberland, *J. Alloys Comp.* **1994**, *210*, 13−17.
[21] W. H. Henley, J. B. Claridge, P. L. Smallwood, H.-C. Zur Loye, *J. Cryst. Growth* **1999**, *204*, 122−127.
[22] A. Varela, K. Boulahya, M. Parras, J. M. Gonzalez-Calbet, T. Vogt, D. J. Buttrey, *Chem. Eur. J.* **2001**, *7*, 1444−1449.
[23] [23a] J. M. Gonzalez-Calbet, A. Varela, K. Boulahya, M. Parras. *Proceedings of 8th European Conference on Solid State Chemistry*, Oslo, **2001**.[23b] J. M. Gonzalez-Calbet, A. Varela, K. Boulahya, M. Parras, *Proceedings of Microscopy*, Barcelona, **2001**, (Ed.: University of Barcelona, 13-36560-2001), p.480.
[24] K. E. Stitzer, M. D. Smith, J. Darriet, H.-C. zur Loye, *Chem. Commun.* **2001**, 1680−1681.
[25] D. Altermatt, I. D. Brown, *Acta Crystallogr., Sect. B* **1985**, *41*, 240−244.
[26] H. M. Rietveld, *J. Appl. Crystallogr.* **1969**, *2*, 65−71.
[27] J. Rodríguez-Carvajal, *J. Physica* **1993**, *B192*, 55−69.

Received October 8, 2001
[I01396]